Generation and use of measurement-based 3-D dose distributions for 3-D dose calculation verification

Robin L. Stern, Benedick A. Fraass, Ansi Gerhardsson,[a] Daniel L. McShan, and Kwok L. Lam
Department of Radiation Oncology, University of Michigan Medical Center, Ann Arbor, Michigan 48109

(Received 22 May 1991; accepted for publication 15 August 1991)

A 3-D radiation therapy treatment planning system calculates dose to an entire volume of points and therefore requires a 3-D distribution of measured dose values for quality assurance and dose calculation verification. To measure such a volumetric distribution with a scanning ion chamber is prohibitively time consuming. A method is presented for the generation of a 3-D grid of dose values based on beam's-eye-view (BEV) film dosimetry. For each field configuration of interest, a set of BEV films at different depths is obtained and digitized, and the optical densities are converted to dose. To reduce inaccuracies associated with film measurement of megavoltage photon depth doses, doses on the different planes are normalized using an ion-chamber measurement of the depth dose. A 3-D grid of dose values is created by interpolation between BEV planes along divergent beam rays. This matrix of measurement-based dose values can then be compared to calculations over the entire volume of interest. This method is demonstrated for three different field configurations. Accuracy of the film-measured dose values is determined by 1-D and 2-D comparisons with ion chamber measurements. Film and ion chamber measurements agree within 2% in the central field regions and within 2.0 mm in the penumbral regions.

Key words: three-dimensional treatment planning, quality assurance, dose verification, photons

I. INTRODUCTION

In recent years, there has been a great deal of work directed toward the creation and use of "three-dimensional" treatment planning systems.[1-10] The term "three dimensional" has been used to describe any number of different capabilities that particular planning systems may contain (see for example a discussion of the various aspects of three dimensionality in Ref. 11). Most workers in the field, however, agree that a "3-D" planning system must be able to calculate the dose to a volume of points (usually arranged in a 3-D grid). Such systems require more wide-ranging testing protocols than do less complex systems.[12] The basic aim of this work is to describe a method to obtain measurement-based 3-D distributions of dose for dose calculation verification and quality assurance for 3-D treatment planning systems.

Basic verification of the accuracy of dose calculations has been discussed by a number of workers.[13-16] In addition, most users of radiation therapy treatment planning systems have themselves performed at least some tests of their systems to convince themselves that the dose calculations presented by the system agree with the data measured at that institution. Dose calculation verification checks are typically performed by comparing calculated and measured doses for either (1) a depth dose curve on the central axis and multiple 1-D profile curves obtained at different depths, or (2) an isodose chart. This comparison is usually performed on the axial plane that contains the beam central axis and is done for a number of different field sizes, SSDs, and other arrangements of the geometry of the beam. In purely 2-D systems, no knowledge of the third dimension is expected,[11] and doses in this central plane are the only doses that matter, since no other effects are expected to be taken into account. In systems that might be characterized by the label "2.5-D",[11] attempts must be made (to some degree) to verify the results in the third dimension as well. In practice, this is most often done by repeating the comparisons of depth dose plus multiple profiles, or an isodose chart, in off-axis axial planes. Sagittal and diagonal profiles are also sometimes used.

This procedure, or variations of it, has been used in nearly all reports of work on quality assurance for planning systems,[17-20] as well as in reports describing the accuracy of dose calculation algorithms.[21] However, the extension of the usual 2-D methods (the use of a series of axial planar dose distributions) to verify or characterize a 3-D dose distribution from a 3-D system has a number of major practical problems. For example, in order to perform checks on the simplest square, open field, a minimal set of checks of a 3-D calculation might include verification in the central axial and two off-axis axial planes, the central sagittal and two off-axis sagittal planes, and both diagonal planes. The simplest way to obtain these doses is probably to measure the central axis depth dose curve and five or more profiles at selected depths for each plane. These profiles for each plane could then be interpolated into 2-D dose distributions on the respective planes. For the square, open field this already results in more than 41 measured curves, if only five depths are used for the profiles. Aside from the time which is required to obtain these curves, one is faced with the additional problem of assuring that each of the more than 40 curves is consistent with each of the other curves, even though they are not all measured at the same time. However, the most important limitation of this kind of approach is that it breaks down for irregularly shaped fields, since there are no longer simple symmetries in the field that allow one to minimize the data needed. In addition, the clinical use of 3-D tools (like beam's

 0094-2405/92/010165-09$01.20

eye view[22]) for field design nearly always results in shaped fields, so that the accuracy and verification of the dose calculations for often heavily blocked fields is extremely important. When one considers the fact that not only open fields, but rectangular and irregularly shaped fields, different SSDs, oblique incidence, irregular surfaces, nonaxial beams, and tissue inhomogeneity situations must be measured and analyzed, it is clear that the traditional methods for verification and measurement can no longer be used.

In this paper, a method for the creation of a complete 3-D dose distribution from measured data is described that does not suffer from the basic problems and limitations mentioned above. It involves the measurement with film of the dose distribution in a series of beam's-eye-view (BEV) planes (planes perpendicular to the beam's central axis and at different depths) along with a single ionization chamber depth dose curve. A divergent interpolation between the planes along beam raylines is used, along with the depth dose curve, to obtain a volumetric dose distribution. Film dosimetry is used to obtain the BEV plane data, since it requires only a small amount of accelerator time and yields the entire planar dose distribution at once. Film has also been shown to be more accurate than an ion chamber for measuring dose in the penumbral regions.[23] In order to minimize difficulties associated with the measurement of megavoltage photon beam depth doses using film, which have been identified with the changing spectral distribution of the beam with depth and the spectral response characteristics of the film,[24,25] ion chamber depth dose data are used to normalize the film data. The effect of the spectral variation across profiles has been shown to have negligible effect on film response for energies up to 6 MV.[23,26] Profiles obtained from film and ionization chamber depth dose data have been used successfully to generate electron beam dose distributions on a plane parallel to the beam containing the central axis.[27]

Below, details of the method used to measure the 2-D BEV planar dose distributions are presented and the method is demonstrated for several different field configurations. To determine the accuracy of the film measurements, comparisons are made to measurements obtained using a scanning ion chamber in a water phantom. Comparisons are made between 1-D dose profiles and 2-D isodose distributions in the BEV planes. Further comparisons are made between ion chamber isodose distributions and those extracted from the 3-D grid of dose generated from the film data in planes perpendicular to the BEV plane (i.e., parallel to the beam axis). Finally, the generated 3-D dose distribution is compared to 3-D calculations, as would be the case for dose calculation verification.

II. MATERIALS AND METHODS

Three different field configurations produced by two different linear accelerators were examined: (1) 10×10-cm^2 open field exposed to 15-MV photons produced by a Clinac 2100C (Varian Associates, Inc., Palo Alto, CA); (2) 15×15-cm^2 field with a central 10×10-cm^2 block exposed to 15-MV photons; and (3) 10×20-cm^2 field with a 60-deg wedge exposed to 6-MV photons produced by a Clinac 1800 (Varian Associates, Inc., Palo Alto, CA). In all cases, the phantom was treated isocentrically (SAD = 100 cm) with an SSD of 90 cm. All data are displayed normalized to 100% at the isocenter (at a depth of 10 cm).

A computer-controlled scanning ion chamber/water phantom system (Wellhofer WP 600C, Wellhofer Dosimetrie Verwaltungs GmbH, Schwarzenbruck, Germany) was used to obtain all ion chamber measurements. Relative dose was measured using a cylindrical ion chamber with active volume of 0.15 cm^3 (model IC 10, Wellhofer Dosimetrie Verwaltungs GmbH, Schwarzenbruck, Germany). An identical chamber was positioned in air near the edge of the field and used as a reference detector to minimize effects of beam variations. Measurements were made in the continuous scanning mode. Depth dose along the central axis and axial and sagittal profiles through the central axis at several depths were measured. For the blocked field, a depth dose and a set of profiles in an off-axis plane outside of the shadow of the block were also taken. In addition, 20 to 50 axial profiles across the BEV planes at depths of d_{max} and 10 cm were measured to derive high-resolution isodose distributions in those planes for comparisons with the film measurements. Even for the planes with the greatest number of profiles, however, the resolution is much better in the axial direction (along the scans) than in the sagittal direction. The smallest spacing between profiles, in the penumbra regions, was never less than 0.2 cm.

All ion chamber dose profile data were smoothed using algorithms provided with the scanner software. A 9-point least-squares smoothing algorithm was used for depth doses, while a 15-point median filter algorithm was used for profiles. Data were converted into an appropriate data format and entered into a 3-D treatment planning system.[4,28] Two-dimensional isodose distributions were then derived by interpolation of profile data. For planes parallel to the beam axis, interpolation was done along divergent beam rays using the depth dose for normalization. For BEV planes, the normalization was based on a sagittal profile through the central axis.

Film measurements were made using Kodak Ready-Pack XV-2 film (Eastman Kodak Co., Rochester, NY) sandwiched between sheets of water-equivalent solid. Two different types of phantom material were used (Model 457 Solid Water, Radiation Measurements, Inc., Middleton, WI and White Water-RW3, Nuclear Associates, Carle Place, NY), but the film pack was always in contact only with the solid water. Film and water-equivalent solid were positioned with their planes perpendicular to the beam central axis. A small hole was punched through one corner of the film, both for use as a position reference and to let all trapped air out of the pack. For each field configuration, films were positioned at several different depths (one at a time) and exposed to approximately the same dose. In addition, a set of films was exposed at constant depth of 10 cm to a range of doses. These latter films were used to derive the film sensitometric curve. All films used for each field configuration were taken from the same box to minimize batch-to-batch variations. Films were then developed in an automatic therapy processor (Model QC-1 R/T, E.I. duPont de Nemours & Co., Inc.,

Wilmington, DE), with all films for each field configuration developed at the same time to minimize variations in processing.

Exposed films were digitized using a laser digitizer (Model DIS 1000, Lumisys Inc., Sunnyvale, CA) with spot size set to 0.42 mm and pixel size 0.45 mm (the maximum available values). To minimize time variations, all films for all three field configurations, including the corresponding sensitometric curve films, were digitized at the same time. Also at that time, a set of digitizer response curves was measured. Since tests of the digitizer had revealed that the output pixel values were dependent on position in the laser beam scanning direction, output pixel values were determined using a calibrated film strip with optical densities ranging from 0.21 to 3.04 which was placed successively at 2-cm intervals across the digitizer stage in the dependent direction. A set of digitizer response curves giving output pixel values as a function of position and true optical density were derived from these measurements. Pixel values for the digitized BEV films were then corrected for positional dependence using these curves.

Film image data files were next converted into the planning system's standard grayscale image file format. When necessary, the number of pixels was reduced using nearest neighbor sampling. The images were entered into the planning system and aligned with the planning system representation of the beam by translating and rotating the coordinate system of the displayed film image. Optical density values were converted to dose values using the appropriate measured film sensitometric curve. A user-variable amount of pixel averaging was applied to this data for better comparison with the ion chamber data. Unless otherwise stated, all film data shown here were smoothed over 0.3 cm in both directions. One-dimensional profiles were extracted and 2-D isodose distributions in the BEV planes were derived from the measured 2-D dose distributions for comparison with ion chamber measurements.

A 3-D dose distribution was then derived for each field configuration. The 2-D BEV plane film-measured dose distributions were first renormalized using the appropriate ion-chamber measured depth dose. Then the volumetric dose matrix was derived by using the ion chamber depth dose curve to interpolate along divergent beam ray lines between adjacent BEV planes of dose. This 3-D dose distribution was then saved in the standard planning system 3-D dose file format. Two-dimensional isodose distributions and 1-D profiles in the BEV and beam-parallel planes were extracted from the volumetric dose distribution for comparison with the ion chamber measurements using utilities within the planning system.

Finally, 3-D calculations were performed[28] for the same field configurations. Comparisons between the 3-D calculations and the generated 3-D dose distributions were performed in three ways: (1) by creating a display in which corresponding isodose lines from the two dose distributions are shown, (2) by creating a dose difference display in which the interpolated data values were subtracted from the calculations, and (3) by creating a dose volume histogram of that difference.

Two additional studies were carried out with BEV plane films. The first tested the reproducibility of digitized film dosimetry measurements. Films were placed at d_{max} in the water-equivalent solid phantom and exposed to a 10×10-cm^2 open 15-MV photon field. Five films were exposed to each of five different doses. As before, all the films were taken from the same box and developed and digitized at the same time. To test for variations in measured dose due to variations in the laser digitizer output for the same real film optical density, two films, exposed to two different doses, were each digitized ten times with the film remaining undisturbed between successive digitizations. Digitized film images were then converted to the planning system image format and entered into the planning system, and the central axis optical density values were determined.

The second study tested the assumption that a film sensitometric curve measured at one depth could be accurately applied to BEV films exposed at different depths. Films were placed one at a time in the BEV planes of an open 10×10 cm^2 15-MV field at four different depths and exposed to a range of doses. Monitor units were adjusted to give approximately the same dose values to the films at each depth. Films were developed, digitized, and entered into the planning system, and the central axis optical density values obtained. Sensitometric curves were then derived for each depth and compared.

III. RESULTS

Data obtained as described above showed good reproducibility for the digitized film dose measurements. Repeated digitizations of the same film yielded a one standard deviation absolute variation in pixel values of 0.005 in optical density units. For the films and dose normalizations presented in this paper, this optical density variation corresponds to a dose variation of approximately 0.3%–0.4%. Pixel values obtained from different films exposed under the same conditions showed a one standard deviation relative variation of $\leqslant 1.5\%$.

The sensitometric curves obtained at four different depths ranging from d_{max} to 20 cm are plotted versus absolute dose in Fig. 1. The largest variation in dose for a given optical density determined from this set of curves is 2.3% at an optical density of approximately 2.3. Variation is less than 1% over most of the measured dose range. This demonstrates that a single sensitometric curve measured at one depth can be accurately used for optical density-to-dose conversion of BEV films at all depths for the experimental situation used here.

The amount of pixel averaging applied to the BEV film data influences the appearance of the derived dose distributions. As the amount of averaging increases, the lines become smoother and the corners of the isodose curves become more rounded. This effect is illustrated in Fig. 2, which shows isodose distributions derived from the film data with different amounts of pixel averaging compared to those derived from the ion chamber measurements. Pixel averaging of the film data corresponds to the spatial averaging that occurs with the scanning ion chamber due to the size of the

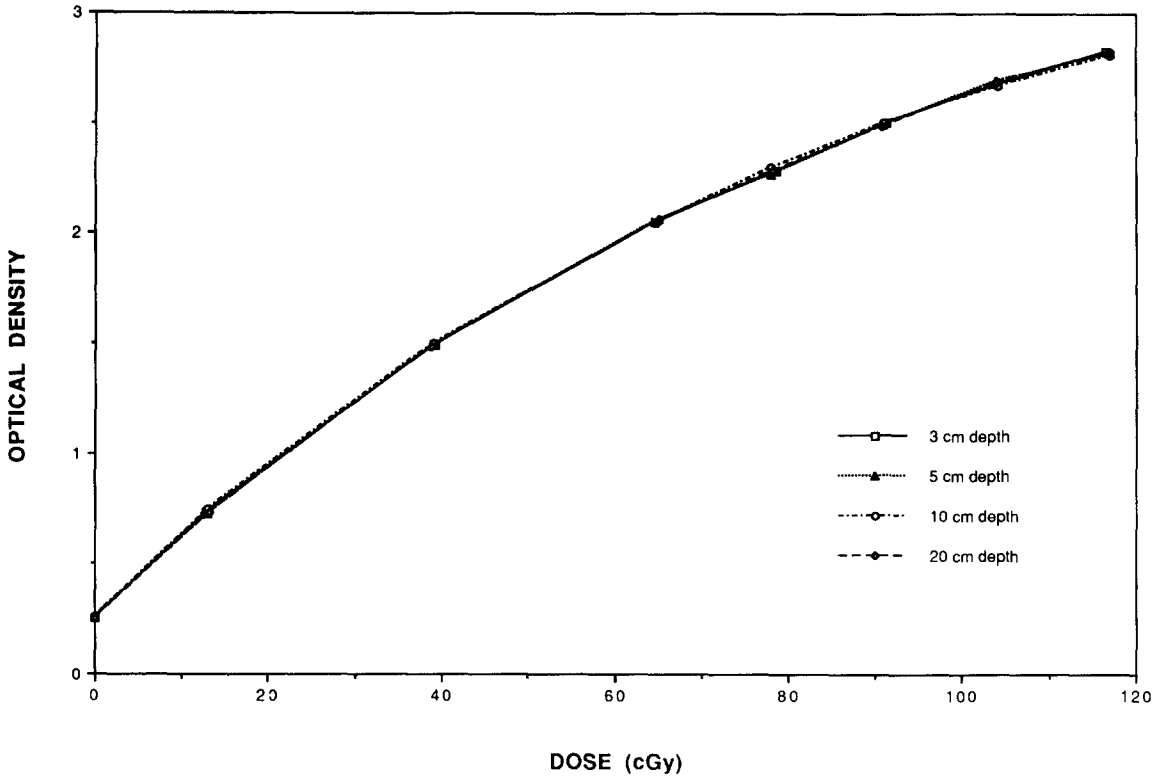

FIG. 1. Film sensitometric curves derived from four sets of BEV films placed at depths of 3, 5, 10, and 20 cm, respectively.

active area of the chamber and its motion. Pixel averaging over 1.0 cm yielded the best overall agreement between the two measurements. For the analysis shown here, a pixel averaging of 0.3 cm was chosen as a good compromise between the high resolution of the film data and the smoothing of small irregular features provided by averaging.

Film-based dose measurements agreed very well with measurements made with the ion chamber. The simplest way to compare the two sets of measurements, and thus determine the relative accuracy of the film dosimetry, was to look at the dose along 1-D profiles. A comparison of the dose

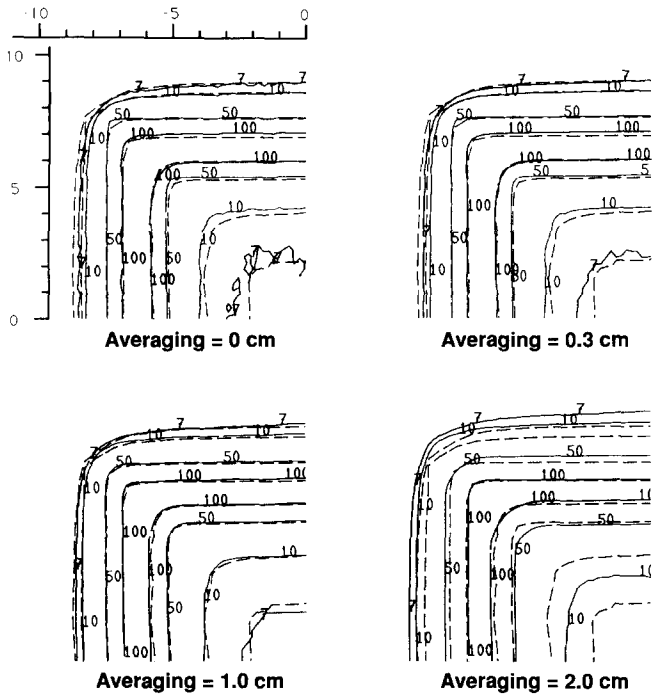

FIG. 2. Isodose distributions in the BEV plane at 10-cm depth for the blocked field derived from film (solid lines) and ion chamber (dashed lines) measurements. The same quadrant of the plane is shown with different amounts of pixel averaging applied to the film data.

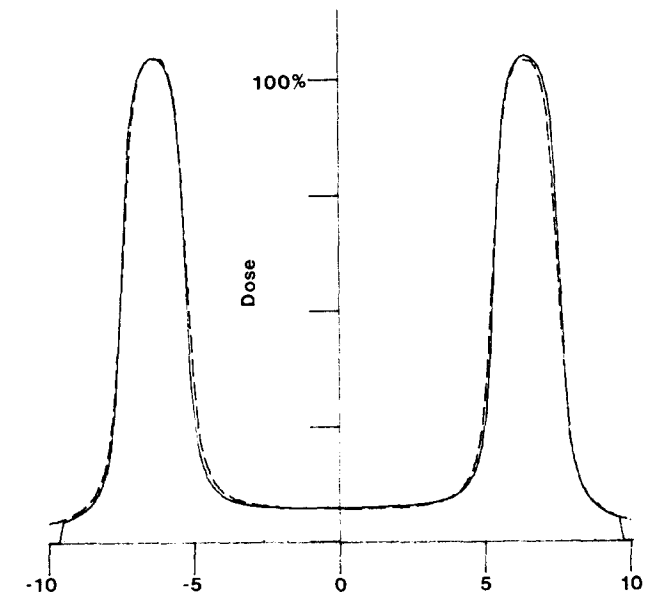

FIG. 3. Central axial profile at 10-cm depth for the blocked field measured by film (solid line) and ion chamber (dashed line), and the difference between the two measurements (dotted line).

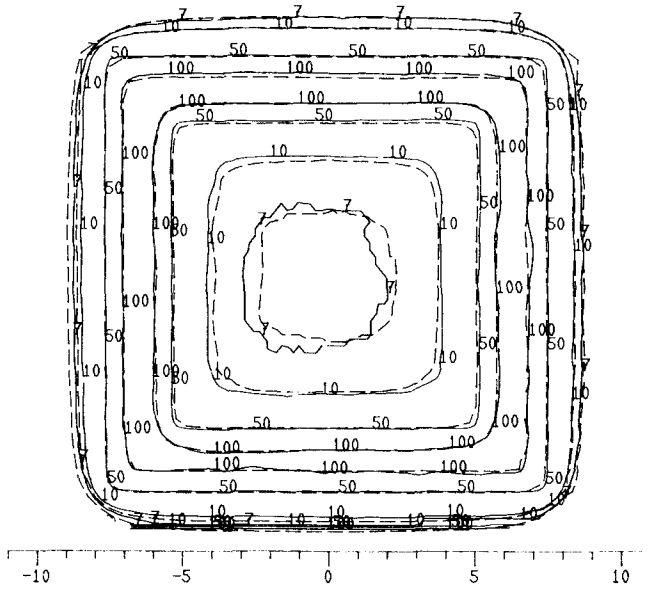

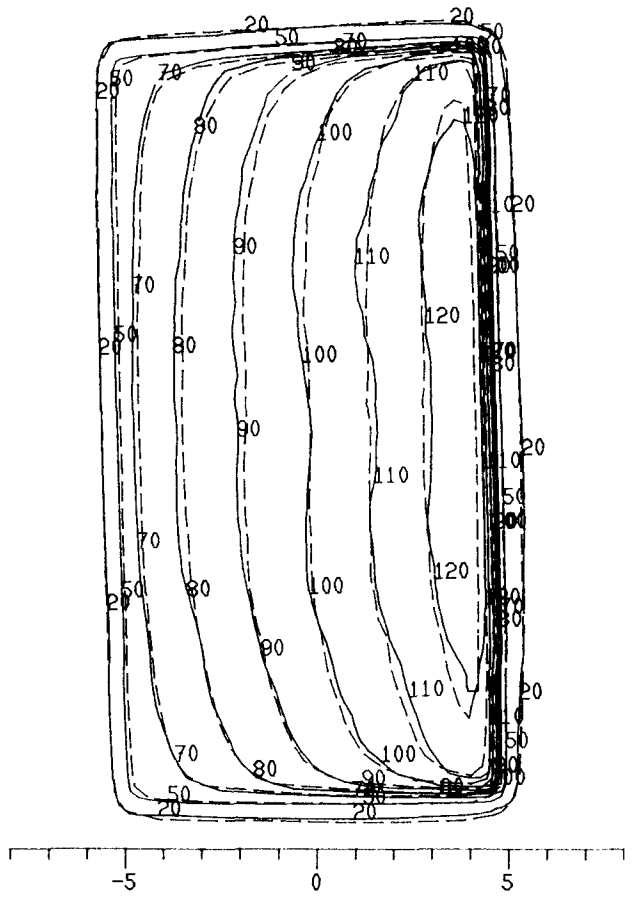

FIG. 4. (a) Isodose distributions in the BEV plane at 10-cm depth for the blocked field derived from film (solid lines) and ion chamber (dashed lines) measurements. (b) Isodose distributions in the BEV plane at 10-cm depth for the wedged field derived from film (solid lines) and ion chamber (dashed lines) measurements.

along the axial profile at 10-cm depth is shown in Fig. 3 for the blocked field case. The difference between the two profiles is also shown. Film and ion chamber measurements are in very good agreement, even in the penumbral regions and under the block.

FIG. 5. 3-D display of the 80% and 140% isodose surfaces derived from the measurement-based 3-D dose distribution for the wedged field.

A way to view more of the data at once is to compare 2-D isodose distributions in the BEV planes. Such comparisons are shown in Figs. 4(a) and (b) for the blocked and wedged fields, respectively.

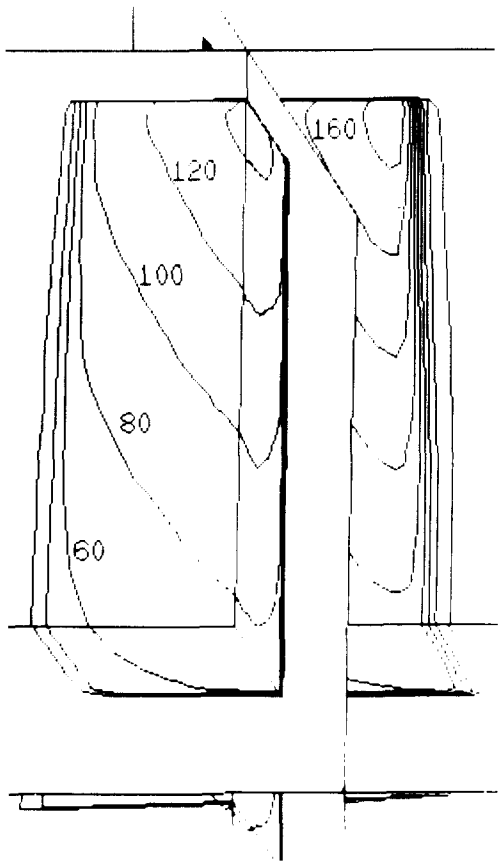

FIG. 6. Axonometric display of the isodose lines from the measurement-based 3-D dose distribution for the wedged field. The central axial and sagittal planes and the BEV plane at a depth of 15 cm are shown.

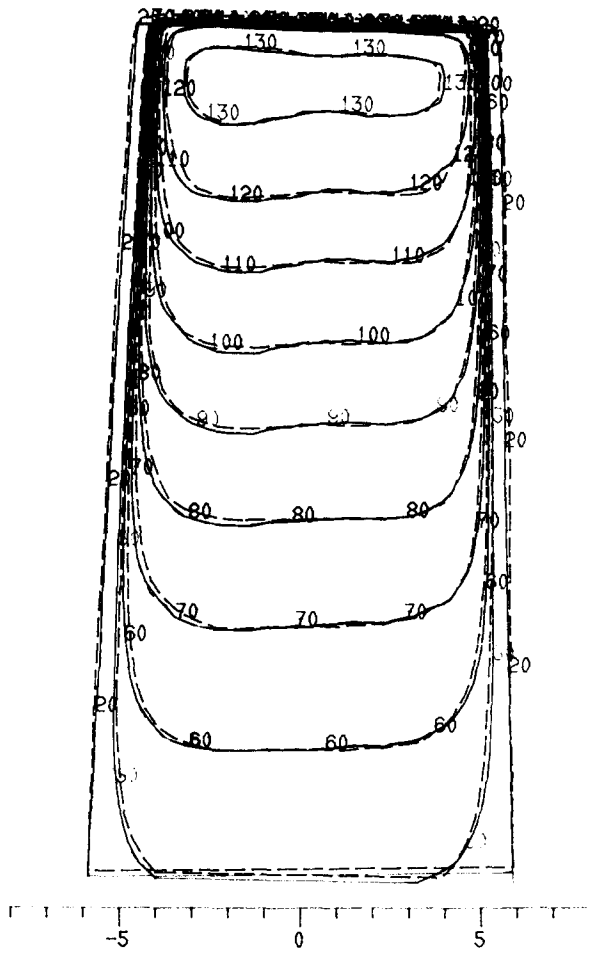

FIG. 7. Isodose distributions in the central axial plane for the open field derived from the measurement-based 3-D dose grid (solid lines) and the ion chamber measurements (dashed lines).

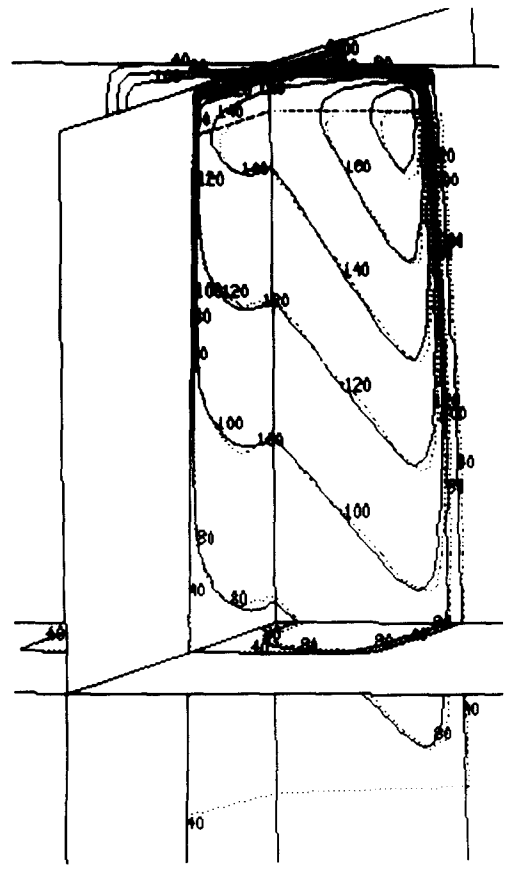

FIG. 8. Axonometric display of the isodose lines from the measurement-based 3-D dose distribution (dotted lines) and the 3-D calculation (solid lines) for the wedged field. The central axial and sagittal planes and the BEV plane at depths of 15 cm are shown.

Figures 3 and 4 show that dose distributions measured with film agree well with those measured with an ion chamber. Within the central high-dose regions of the fields studied here, variation in normalized dose between the two sets of measurements was generally $\leqslant 2\%$. Larger variations are typically due to artifacts in the ion chamber dose distributions due to grid size effects and interpolation and profile normalization effects. In the penumbral regions, the maximum positional difference was 2.0 mm, with the difference usually $\leqslant 1.0$ mm. Since the field sizes were set separately for each set of measurements, these positional differences include the accuracy of the field size setting. These differences can be ascribed to the ion chamber size (partially compensated for by pixel averaging the film data) and the effect of the loss of charged particle equilibrium in the penumbra on the ionization-to-dose conversion for the chamber data.[23] The good agreement between film and ion chamber dose measurements throughout the BEV planes for both photon energies used indicates that the effects of spectral variations across the beam are small and can be disregarded. The values given apply to the 2-D film measurements in comparison with the ion chamber measurements. The generated 3-D dose grid values are expected to have slightly less agreement due to additional interpolation and grid effects.

Three-dimensional dose grids were interpolated from the BEV film data for all three field configurations. There are many ways to display this information. Figure 5 shows a 3-D display of two isodose surfaces for the wedged field. Figure 6 shows an axonometric display for the same field. The axial and sagittal planes through the central axis and the BEV plane at 15-cm depth are shown.

In order to compare the generated 3-D dose grid with ion chamber measurements, 1-D or 2-D dose or 2-D isodose distributions must be extracted from the 3-D dose distributions. Planes orthogonal to the original BEV planes give the best indication of the consistency of the 3-D interpolation. Figure 7 shows isodose lines derived from the two different dose distributions on the central axial plane for the open field.

The ultimate purpose of these measurements is for comparison to 3-D dose calculations. Figure 8 shows isodose lines derived from the film-based generated dose grid compared with the calculated isodose lines[28] for the wedged field case. Again, the central axial and sagittal planes and the BEV plane at 15-cm depth are shown. A 3-D dose difference matrix was calculated by subtracting the data-based generated dose values from the calculation. The differential dose volume histogram for this dose difference (Fig. 9) is used to summarize the agreement between the calculated and measurement-based distributions.

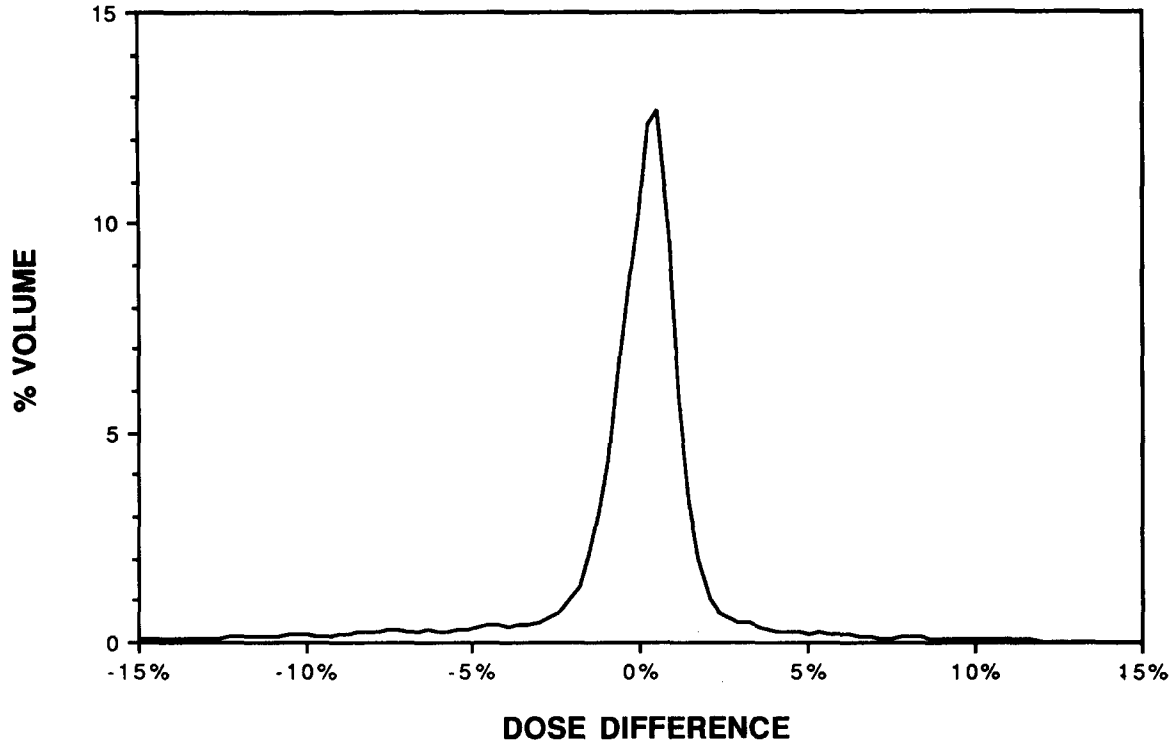

FIG. 9. Differential dose volume histograph of the difference between the measurement-based 3-D dose distribution and the 3-D calculation within the 20% isodose surface for the wedged field. The plotted dose difference is the absolute difference between the two normalized distributions.

IV. DISCUSSION

Dose calculation algorithm verification and quality assurance for 3-D treatment planning require a practical method for the generation of measurement-based dose distributions for a full three-dimensional volume. Although the usual 2-D methods of data acquisition and analysis may possibly be practical and useful for the simplest experimental situations, their application to the complex situations which are typically used in 3-D treatments (e.g., heavily shaped fields, nonaxial dose distributions, and beam directions) is extremely problematic. Rather than rely on simple sets of 1-D and 2-D measurements to perform dose verification comparisons on simple experimental situations, the divergent interpolation used to create the 3-D measurement-based dose distribution makes use of the facts that (1) along ray lines the beam geometry is constant between all planes and (2) the relationship of doses at different depths is controlled by the physics of the interaction between the radiation and the phantom material. This is not true for interpolation between planes parallel to the beam, where there are no physical laws defining where beam and block edges must be in the field.

The use of full planes of data measured with film (BEV planes perpendicular to the axis of the beam) along with depth doses measured with an ion chamber to assure accurate interpolation between BEV planes should allow these techniques to be easily extended to most kinds of measurements which are needed in homogeneous phantoms. This includes many of the experimental situations of interest for 3-D dose calculation verifications, including fields shaped with blocks or multileaf collimators, irregular surface contours, oblique field incidence, and other situations. Further work will clearly be needed to extend this method to the very important area of 3-D measurements and calculations in phantoms with significant and irregular inhomogeneities.

The present method has also been developed with another series of issues in mind: the verification of dose distributions obtained through computer-controlled conformal therapy. There is a great deal of interest in the computer-controlled devices like multileaf collimators,[29] use of "dynamic wedges,"[30,31] the use of segmental conformal therapy (treatment of multiple fixed field segments under automatic computer control), and the use of computer controlled scanned photon and electron beams[32] which can even allow some modulation of the beam intensity across the field. Investigation of each of these kinds of treatment techniques will often require full 3-D dose verifications and at the same time will require the use of an integrating dosimetry sensor (like film). The combination of the use of film and the 3-D interpolation of the measured data solves many of the immediate problems associated with the dose verification and characterization of any of these new and exciting technologies. These techniques also will be extremely useful for daily quality assurance checks of machines with computer-controlled conformal therapy capability, particularly ones with scanned photon and/or electron beams.

Although it is important to use great care with the film dosimetry method used here, the method removes the largest problems typically associated with use of film. The use of ionization chamber depth dose data for normalization of each individual film, and as a basis for the dose interpolation between BEV planes, removes the dependence of the results

on accurate depth dose behavior of the film. If large energy spectrum changes are expected to affect the film data at different depths, then individual optical density to dose conversions could be determined at each depth in the phantom, although this has not been necessary in this work. The use of the laser film digitizer, with 0.5-mm spot size, means that the measurements do not include size effects like those which typically result from the use of an ion chamber in a water phantom system or a large-spot-size scanning film densitometer. In fact, extra pixel averaging was necessary in order to degrade the film resolution in order to compare to the ion chamber data.

One of the major advantages of film dosimetry over ion chamber measurements is the savings in time, particularly accelerator time. For example, it takes about the same amount of time, depending on the field size, to obtain an entire set of BEV plane and sensitometric curve films as it does to measure with an ion chamber either the limited set of axial, sagittal, and diagonal profiles described in the Introduction or a single BEV plane with spatial resolution of 0.2–0.3 cm. Therefore, it would take 4 to 5 times longer to take the data needed to derive the 3-D grid of dose using the scanning ion chamber than film. Furthermore, setup and take-down time is less with film. Film dosimetry thus offers a substantial savings in the amount of time needed on the accelerator for data acquisition. The savings of physicists' time is maintained through the data analysis work, since it takes roughly the same amount of time to process the film and create the data-based 3-D dose distribution as it does to enter 1-D profile and depth dose data and use them for standard 2-D dose verifications on axial and sagittal planes. An additional savings of both accelerator time and data processing time can be realized by applying the method of Mota *et al.* to linearize film sensitometric curves for relative dosimetry.[33] Use of this method would eliminate the need to derive a separate sensitometric curve for each set of BEV film measurements.

One of the more significant causes of inaccuracy in the present work was the inability to automatically align the film data to the experimental situation inside the planning system. This was especially important in the wedged field case, since the edges of the BEV dose distributions were more difficult to use for alignment. In order to remove this difficulty, the manual graphical alignment of each BEV film dose distribution to the beam shape will be automated, using edge tracking tools as well as using a film cassette with fiducial marks to aid alignment.

Substantial hardware and software capabilities are required to implement this technique. A film digitizer is needed, along with a way of transferring data from digitizer to planning system. A scanning densitometer could be used instead of the film digitizer but would be much more time consuming and would yield data of reduced spatial resolution. A high-definition graphics display device is needed for review and alignment of the film data. Software requirements include the ability to handle 2-D and 3-D dose distributions, the ability to generate and use dose distributions based on data rather than on calculations, the ability to perform interpolation in three dimensions between planes along divergent beam lines, and the ability to extract lines and planes from 3-D dose distributions. Features such as 3-D histograms and 3-D dose difference distributions are likely to be one of the more important ways to communicate and analyze the comparison between the calculated and measured data. Finally, various 3-D display tools and 2-D hard copy output techniques are important in order to allow real analysis and review of the comparisons.

V. CONCLUSIONS

The evolution of computerized treatment planning has led to very complex systems that perform calculations in a three-dimensional space. These systems require well defined dose calculation verification techniques. Traditional 2-D methods of measurement using depth doses and selected profiles cannot practically be applied in the 3-D situation. We have demonstrated a new method of deriving a 3-D volume of photon dose values based on BEV film dosimetry and using interpolation along divergent ray lines. A depth dose measured with an ion chamber is used for renormalization to avoid inaccuracies due to the changing spectral characteristics of the beam with depth. Overall accuracy of this method compares well with the data obtained with a standard scanning ion chamber/water phantom system. The generated 3-D grid of dose can then be compared to 3-D dose calculations to allow for the first time a true analysis of the accuracy of 3-D volume dose calculations.

[a] Present address: Department of Radiation Physics, Karolinska Institute, University of Stockholm, Stockholm, Sweden.

[1] M. Goitein and A. Mark, "Multi-dimensional treatment planning. I. Delineation of anatomy," Int. J. Radiat. Oncol. Biol. Phys. **9**, 777–787 (1983).

[2] M. Goitein, M. Abrams, D. Rowell, H. Pollari, and J. Wiles, "Multi-dimensional treatment planning. II. Beam's-eye-view, back projection, and projection through CT sections," Int. J. Radiat. Oncol. Biol. Phys. **9**, 789–797 (1983).

[3] L. M. Chin, R. L. Siddon, G. K. Svensson, and C. Rose, "Progress in 3-D treatment planning for photon beam therapy," Int. J. Radiat. Oncol. Biol. Phys. **11**, 2011–2020 (1985).

[4] B. A. Fraass and D. L. McShan, "3-D treatment planning: I. Overview of a clinical planning system," in *The Use of Computers in Radiation Therapy*, edited by I. A. D. Bruinvis, P. H. van der Giessen, H. J. van Kleffens, and F. W. Wittkamper (Elsevier, Amsterdam, 1987), pp. 273–276.

[5] M. R. Sontag, M. D. Altschuler, P. Bloch, R. A. Reynolds, R. E. Wallace, and G. K. Waxler, "Design and clinical implementation of a second generation three-dimensional treatment planning system." in Ref. 4, pp. 285–288. Giessen, H. J. van Kleffens, and F. W. Wittkamper (Elsevier, Amsterdam, 1987), pp. 285–288.

[6] G. W. Sherouse, C. E. Mosher, Jr., K. Novins, J. Rosenman, and E. L. Chaney, "Virtual simulation: concept and implementation," in Ref. 4, pp. 433–436.

[7] R. Mohan, G. Barest, L. J. Brewster, C. S. Chui, G. J. Kutcher, J. S. Laughlin, and Z. Fuks, "A comprehensive three-dimensional radiation treatment planning system," Int. J. Radiat. Oncol. Biol. Phys. **15**, 481–495 (1988).

[8] J. Rosenman, G. W. Sherouse, H. Fuchs, S. M. Pizer, A. L. Skinner, C. Mosher, K. Novins, and J. E. Tepper, "Three-dimensional display techniques in radiation therapy treatment planning," Int. J. Radiat. Oncol. Biol. Phys. **16**, 263–269 (1989).

[9] J. Jacky, "3-D radiation therapy treatment planning: overview and assessment," Am. J. Clin. Oncol. **13**, 331–343 (1990).

[10] T. Nishida, Y. Nagata, M. Takahashi, M. Abe, N. Yamaoka, H. Ishihara, Y. Kubo, H. Ohta, and C. Kazusa, "CT simulator: A new 3-D planning and simulating system for radiotherapy: Part I. Description of system," Int. J. Radiat. Oncol. Biol. Phys. **18**, 499–504 (1990).

[11] B. A. Fraass and D. L. McShan, "Developments in radiation therapy

treatment planning", in *Computers in Medical Physics*, edited by A. R. Benedetto, H. K. Huang, and D. P. Ragan (American Institute of Physics, Woodbury, NY, 1990), pp. 303–315.

[12] A. Gerhardsson, B. A. Fraass, D. L. McShan, and R. K. Ten Haken, "Development of quality assurance tests for 3-D treatment planning," Med. Phys. **16**, 673 (1989).

[13] E. C. McCullough and A. M. Krueger, "Performance evaluation of computerized treatment planning systems for radiotherapy: external photon beams," Int. J. Radiat. Oncol. Biol. Phys. **6**, 1599–1605 (1980).

[14] C. F. Westmann, B. J. Mijnheer, and H. J. van Kleffens, "Determination of the accuracy of different computer planning systems for treatment with external photon beams," Radiother. Oncol. **1**, 339–347 (1984).

[15] O. Sauer, G. Nowak, and J. Richter, "Accuracy of dose calculations of the Philips treatment planning system OSS for blocked fields, in Ref. 4, pp. 57–60.

[16] C. Burman, G. J. Kutcher, M. Hunt, L. Brewster, and R. Mohan, "Acceptance testing criteria for a CT based 3D treatment planning system," Med. Phys. **16**, 465 (1989).

[17] AAPM Task Group 21, "A protocol for the determination of absorbed dose from high-energy photon and electron beams," Med. Phys. **10**, 1–31 (1983).

[18] D. Lepinoy, P. Aletti, G. Boisserie, H. Bouhnick, G. Estrade, M. T. Hoornaert, J. C. Horiot, P. Piret, A. Piron, C. Redon, and J. C. Rosenwald, "Quality assurance program for computers in radiotherapy: Progress report," in *Proceedings of the Eight International Conference on the Use of Computers in Radiation Therapy* (IEEE Computer Society, Silver Spring, MD, 1984), pp. 322–327.

[19] U. F. Rosenow, H.-W. Dannhausen, K. Lubbert, F. Nusslin, J. Richter, B. Robrandt B, W.-W. Seelentag, and H. Wendhausen, "Quality assurance in treatment planning. Report from the German Task Group," in Ref. 4, pp. 45–58.

[20] R. W. Wittkamper, B. J. Mijnheer, and H. J. van Kleffens, "Dose intercomparison at the radiotherapy centers in The Netherlands. 2. Accuracy of locally applied computer planning systems for external photon beams," Radiother. Oncol. **11**, 405–414 (1988).

[21] A. S. Shui and K. R. Hogstrom, "A pencil-beam redefinition algorithm for electron dose distribution," in Ref. 4, pp. 69–72.

[22] D. L. McShan, B. A. Fraass, and A. S. Lichter, "Full integration of the beam's eye view concept into computerized treatment planning," Int. J. Radiat. Oncol. Biol. Phys. **18**, 1485–1494 (1990).

[23] C. H. Sibata, H. C. Mota, A. S. Beddar, P. D. Higgins, and K. H. Shin, "Influence of detector size in photon beam profile measurements," Phys. Med. Biol. **36**, 621–631 (1991).

[24] D. W. Anderson and F. St. George, "Comparison of film and ion chamber systems for depth-dose measurements for a 25 MV beam," Phys. Med. Biol. **24**, 636–638 (1979).

[25] J. F. Williamson, F. M. Khan, and S. C. Sharma, "Film dosimetry of megavoltage photon beams: a practical method of isodensity-to-isodose curve conversion," Med. Phys. **8**, 94–98 (1981).

[26] R. K. Rice, J. L. Hansen, G. K. Svensson, and R. L. Siddon, "Measurements of dose distributions in small beams of 6 MV x-rays," Phys. Med. Biol. **32**, 1087–1100 (1987).

[27] A. S. Shui, V. A. Otto, and K. R. Hogstrom, "Measurement of dose distributions using film in therapeutic electron beams," Med. Phys. **16**, 911–915 (1989).

[28] B. A. Fraass, D. L. McShan, R. K. Ten Haken, and K. M. Hutchins, "3-D treatment planning: V. A fast 3-D photon calculation model," in Ref. 4, pp. 521–524.

[29] P. Kallman, B. Lind, A. Eklof, and A. Brahme, "Shaping of arbitrary dose distributions by dynamic multileaf collimation," Phys. Med. Biol. **33**, 1291–1300 (1988).

[30] P. K. Kijewski, L. M. Chin, and B. E. Bjarngard, "Wedged-shaped dose distributions by computer-controlled collimator motion," Med. Phys. **5**, 426–429 (1978).

[31] D. D. Leavitt, M. Martin, J. H. Moeller, and W. L. Lee, "Dynamic wedge field techniques through computer-controlled collimator motion and dose delivery," Med. Phys. **17**, 87–91 (1990).

[32] A. Brahme, T. Kraepelien, and H. Svensson, "Electron and photon beams from a 50 MeV racetrack microtron," Acta Radiolog. Oncol. **19**, 305–319 (1980).

[33] H. C. Mota, C. H. Sibata, W. Roberts, and P. D. Higgins, "Film dosimetry: linearization of dose-response for relative measurements of dose distributions," Phys. Med. Biol. **35**, 565–569 (1990).